Journal of the Nigerian Association of Mathematical Physics
Volume 62, (October – Dec., 2021 Issue), **pp147 – 152**

FLEXURAL CHARACTERISTICS OF HOLLOW CORED RECTANGULAR PLAIN CONCRETE BEAMS USING FINITE ELEMENT APPROACH

O.U. Orie and U.K. Ogbonna*

Civil Engineering Department, Universityof Benin, Benin City, Nigeria.

Abstract

In this paper, the flexural characteristics of Hollow-Cored Reinforced Concrete Beams point loaded at mid-span were investigated analytically and numerically. Finite element numerical approach was used to examine the hollow cored beams using isoparametric geometric transformation of their coordinates to discretize the Hollow-Cored Beam section numerically. A 9-noded Lagrangian quadratic element for the rectangular section and an 8-noded Serendipity cubic element for the circular-hollow section were used to create shape functions at each node. Double integration of the equations relating the shape functions and the Jacobian determinant with respect to the reference coordinates was used to compute the moment of inertia numerically. Numerical solutions to the governing matrix equations linking deflection and ultimate load were also obtained. The analytical and numerical results were found to be in agreement with the literature. The paper concluded that using finite element numerical approach the moment of inertia and the ultimate failure loads of the hollow-cored beams increases with an increase in diameter of the hollow core beam while the deflection increased as the diameter of the hollow core increased up to 30mm, beyond which the deflection dropped.

Keywords: Concrete, Beams, Flexure, Analytical method and Numerical method

1.0 Introduction

A hollow core beam is a horizontal structural member having a void running through its longitudinal axis and is designed to carry load principally in the flexure direction. As a result, in order to ensure their structural integrity, their structural behavior must be investigated. Hollow cores provide greater flexural strength and stiffness than solid members [1]. All analysis methods, according to [2] can be divided into three categories: experimental, analytical, and numerical methods. Because specialized equipment, testing facilities, and other resources are required, experimental approaches are the most dependable, but they are also the most expensive. Analytical methods are also reliable, but they are time consuming and inconvenient for high levels of accuracy. The finite element numerical method is a numerical procedure that can be used to solve a variety of engineering problems by replacing any structure with a finite number of elements connected at a finite number of nodal points [3]. Numerical approaches are easy and do not require any laboratory setup, despite the fact that they yield only approximate results [1]. Investigated the influence of altering effective flange width and hollow core position in the compression zone of a plain concrete beam with a point load at midspan on the hollow concrete's optimal cored section of a hollow concrete beam. While maintaining a constant cross-sectional area and varying the section dimensions randomly in steps of 10mm from 150mm to 190mm flange width, equations were derived using the double integration method to determine the moment of inertia of the sections and corresponding deflections as the load increased up to failure. The acquired results were compared to experimental results that had been linearized. The results showed that as the flange width rose, the deflection with failure loads of the beam samples increased. The flexural behavior of a rectangular reinforced concrete hollow beam with a polypropylene plastic sheet filling was investigated by [4]. Because concrete is weak in tension and strong in compression, steel is used in the tension zone to take tensile loads. As a result, the tension zone's strength is ignored in comparison to the compression zones. As a result, no concrete should be used in the tension zone. However, between the compression and tension zones, this concrete works as a strain or stress transfer medium. However, because concrete below or around the

Corresponding Author**:** Ogbonna U.K., Email: engrogbonnaku@gmail.com, Tel: +2348147699692

neutral axis is underutilized, any light-weight or waste material can be used to replace it. The findings of the beam tests revealed that as the percentage of replacement increases, the flexural strength of the beam drops, and the deflection of the beam reduces in comparison to the control beam [5]. Experiments and numerical simulations were used to investigate the influence of a non-uniform reinforcement ratio along the length of the beam on flexural behavior. Four reinforced concrete beams with varying reinforcing ratios were used in the experiment. In the constant moment zone, however, three of the four beams had the same reinforcement ratio (0.012). During the test, the cracking load, load carrying capacity, and deflection were all measured. In order to model the experimental behavior, nonlinear finite element software was used. After that, a parametric investigation was carried out. It was discovered that the tension stiffening of reinforced concrete beams is determined by the concrete area in the tension zone, rather than the reinforcement ratio. The behavior of reinforced concrete beams was predicted precisely using Finite Element Analysis (FEA). A parametric study was developed by [6] based on a real-scale model experimental program in order to assess the vibration performance of prestressed hollow-core slab system on spans larger than those on which tests were conducted, as well as the interaction between the concrete poured in different stages. Abaqus 6.11 finite element software was used to perform the experimental measurements and conduct the investigation. The simulations were carried out by expanding the slab's span in order to observe the fundamental frequency variation. In addition, numerous types of concrete topping thickness were used in the simulations.

2.0 Methodology

Using a finite element method, the flexural characteristics of hollow cored rectangular plain concrete beams point loaded at mid-span are investigated. Finite element, finite difference, stiffness, energy, and double integration are some of the beam analysis approaches [1]. The finite element approach was chosen for this project because it is well-suited to the task and allows for the discretization of the sectional properties of the beam section via isoparametric geometric transformations of their coordinates. A 9-noded Lagrangian quadratic element and an 8-noded Serendipity cubic element were given shape functions at each node. The moment of inertia about the cross section's centroidal axis, which runs parallel to the neutral axis, was investigated using double integration and equations linking shape functions, discretized nodal point coordinates, and the Jacobian matrix's determinant. The deflection of the hollow cored Beam sections was calculated analytically and numerically after they were loaded at mid-span with a load increment of 1KN intervals. The ultimate load data was adopted from the work of [7] who applied the parallel axis theorem to calculate the moment of inertia of the rectangular and circular-hollow core beam section about the centroidal axis of the cross section which the neutral axis runs along. Three types of Beam sections were investigated as shown in Table 4.1.

3.0 Background Theory

The moment of inertia of each component area around the centroidal axis of the cross section, which the neutral axis runs, was calculated using the parallel axis theorem. The discretized beam section's moment of inertia was calculated numerically by geometric transformation of the hollow cored beam section. The simple geometry of the reference element (η, ξ,) is transferred to the geometry of the real element (y, z) via a transformation that defines the coordinates of each point in the real domain in terms of the coordinates of the corresponding point in the reference domain [8]. The double integration method for deflection of beams was used to derive the equation for the deflection at mid span which is the point for maximum bending for the simply supported beam point loaded at mid span by developing beam stiffness matrix and load-displacement matrix [7].

3.1 Numerical Load-deflection equation

From the y, z coordinates of the nodes of the rectangular section, the Jacobian matrix is given by: [9]

$$J = \begin{bmatrix} \frac{\partial N_1}{\partial \xi} & \frac{\partial N_2}{\partial \xi} & \frac{\partial N_3}{\partial \xi} & \frac{\partial N_4}{\partial \xi} & \frac{\partial N_5}{\partial \xi} & \frac{\partial N_6}{\partial \xi} & \frac{\partial N_7}{\partial \xi} & \frac{\partial N_8}{\partial \xi} & \frac{\partial N_9}{\partial \xi} \\ \frac{\partial N_1}{\partial \eta} & \frac{\partial N_2}{\partial \eta} & \frac{\partial N_3}{\partial \eta} & \frac{\partial N_4}{\partial \eta} & \frac{\partial N_5}{\partial \eta} & \frac{\partial N_6}{\partial \eta} & \frac{\partial N_7}{\partial \eta} & \frac{\partial N_8}{\partial \eta} & \frac{\partial N_9}{\partial \eta} \end{bmatrix} \begin{bmatrix} y_1 & z_1 \\ y_2 & z_2 \\ y_3 & z_3 \\ y_4 & z_4 \\ y_5 & z_5 \\ y_6 & z_6 \\ y_7 & z_7 \\ y_8 & z_8 \\ y_9 & z_9 \end{bmatrix} \quad (1)$$

The Jacobian determinant becomes

$$|J| = J_{11} J_{22} - J_{12} J_{21} \quad (2)$$

The determinant |J| can be expressed in terms of the shape function derivatives and the element nodal coordinate vectors as

$$| J | = \frac{\partial N}{\partial \eta} y \frac{\partial N}{\partial \zeta} z - \frac{\partial N}{\partial \eta} z \frac{\partial N}{\partial \zeta} y \quad (3)$$

The geometrical transformation for the nine-node lagrangian element is defined in terms of the shape function below: [10]
For ξ = -1, 0, or + 1 and η = -1, 0, or + 1,
Where
η and ξ are the axis of the reference domain, and
The local node numbers 1, 2, and 3 on this axis correspond to locations ξ = -1, 0, and +1

$$N_1 = \frac{\eta\xi(1-\xi)(1-\eta)}{4}, N_2 = \frac{\eta\xi(1+\xi)(1-\eta)}{4}, N_3 = \frac{\eta\xi(1+\xi)(1+\eta)}{4}$$
$$N_4 = \frac{-\eta\xi(1-\xi)(1+\eta)}{4}, N_5 = \frac{-\eta(1-\eta)(1-\xi)(1+\xi)}{2}, N_6 = \frac{\xi(1-\eta)(1+\eta)(1+\xi)}{2}$$
$$N_7 = \frac{\eta(1+\eta)(1-\xi)(1+\xi)}{2}, N_8 = \frac{-\xi(1-\eta)(1+\eta)(1-\xi)}{2}, N_9 = (1-\xi)^2(1-\eta)^2 \quad (4)$$
$$\frac{\partial N_1}{\partial \eta} = \frac{\xi(1-2\eta)(1-\xi)}{4}, \frac{\partial N_2}{\partial \eta} = \frac{-(1-2\eta)(1-\xi)}{2}, \frac{\partial N_3}{\partial \eta} = \frac{-\xi(1-2\eta)(1+\xi)}{4}$$
$$\frac{\partial N_4}{\partial \eta} = 4\eta\xi(1-\xi), \frac{\partial N_5}{\partial \eta} = -8\eta(1-\xi^2), \frac{\partial N_6}{\partial \eta} = -4\eta\xi(1+\xi)$$
$$\frac{\partial N_7}{\partial \eta} = -\xi(1+2\eta)(1-\xi), \frac{\partial N_8}{\partial \eta} = 2(1+2\eta)(1-\xi^2), \frac{\partial N_9}{\partial \eta} = \xi(1+2\eta)(1+\xi) \quad (5)$$

Similarly,
$$\frac{\partial N_1}{\partial \xi} = \frac{\eta(1-\eta)(1-2\xi)}{4}, \frac{\partial N_2}{\partial \xi} = \eta\xi(1-\eta), \frac{\partial N_3}{\partial \xi} = \frac{-\eta(1-\eta)(1+2\xi)}{4}$$
$$\frac{\partial N_4}{\partial \xi} = \frac{-(1-\eta^2)(1-2\xi)}{2}, \frac{\partial N_5}{\partial \xi} = -2\xi(1-\eta^2), \frac{\partial N_6}{\partial \xi} = \frac{(1-\eta^2)(1+2\xi)}{2}$$
$$\frac{\partial N_7}{\partial \xi} = \frac{-\eta(1+\eta)(1-2\xi)}{4}, \frac{\partial N_8}{\partial \xi} = -\eta\xi(1+\eta), \frac{\partial N_9}{\partial \xi} = \frac{\eta(1+\eta)(1+2\xi)}{4} \quad (6)$$

The geometrical transformation for the 8-noded quadratic Cubic Serendipity element is defined in terms of the shape function below: [10].
For ξ = -1, 0, or + 1 and η = -1, 0, or + 1,

$$N_1 = \frac{-(1-\xi)(1-\eta)(1+\xi+\eta)}{4}, N_2 = \frac{-(1+\xi)(1-\eta)(1-\xi+\eta)}{4}, N_3 = \frac{-(1+\xi)(1+\eta)(1-\xi-\eta)}{4}$$
$$N_4 = \frac{-(1-\xi)(1+\eta)(1+\xi-\eta)}{4}, N_5 = \frac{(1-\xi^2)(1-\eta)}{2}, N_6 = \frac{(1+\xi)(1-\eta^2)}{2}$$
$$N_7 = \frac{(1-\xi^2)(1+\eta)}{2}, N_8 = \frac{(1-\xi)(1-\eta^2)}{2}, \quad (7)$$
$$\frac{\partial N_1}{\partial \eta} = \frac{-(-\xi+\xi^2-2\eta+2\eta\xi)}{4}, \frac{\partial N_2}{\partial \eta} = \frac{-(\xi-\xi^2-2\eta-2\eta\xi)}{4}, \frac{\partial N_3}{\partial \eta} = \frac{-(-\xi-\xi^2-2\eta-2\eta\xi)}{4}$$
$$\frac{\partial N_4}{\partial \eta} = \frac{-(\xi-\xi^2-2\eta+2\eta\xi)}{4}, \frac{\partial N_5}{\partial \eta} = \frac{(-1+\xi^2)}{2}, \frac{\partial N_6}{\partial \eta} = \frac{(1-\eta^2)}{2},$$
$$\frac{\partial N_7}{\partial \eta} = \frac{(1-\xi^2)}{2}, \frac{\partial N_8}{\partial \eta} = -\eta(-1+\xi) \quad (8)$$
$$\frac{\partial N_1}{\partial \xi} = \frac{-(-2\xi+2\xi\eta+\eta^2)}{4}, \frac{\partial N_2}{\partial \xi} = \frac{-(\eta-2\xi+2\xi\eta-\eta^2)}{4}, \frac{\partial N_3}{\partial \xi} = \frac{-(-2\xi-2\xi\eta-\eta^2-\eta)}{4}$$
$$\frac{\partial N_4}{\partial \xi} = \frac{-(\eta-2\xi-2\xi\eta+\eta^2)}{4}, \frac{\partial N_5}{\partial \xi} = (-1+\eta), \frac{\partial N_6}{\partial \xi} = \frac{(1-\eta^2)}{2}$$
$$\frac{\partial N_7}{\partial \xi} = -\xi(1+\eta), \frac{\partial N_8}{\partial \xi} = \frac{(-1+\eta^2)}{2} \quad (9)$$

The moment of inertia of the transformed rectangular section and the transformed circular section is given by the following equations respectively according to [11]

$$I_R = \sum_{e=1}^{2} \int_{-1}^{1}\int_{-1}^{1} (Nz_e)^2 |J_e| d\eta\, d\xi \quad (10)$$
$$I_C = \sum_{e=1}^{2} \int_{-1}^{1}\int_{-1}^{1} (Ny_e)^2 |J_e| d\eta\, d\xi \quad (11)$$

Where
N = Shape function
y_e = y coordinate of the nodal point of the physical domain
z_e = z coordinate of the nodal point of the physical domain
$|J_e|$= the determinant of the Jacobian matrix

Equations (10) and (11) after some substitution, simplifications and rearrangements leads to

$$I_R = \sum_{e=1}^{2} \int_{-1}^{1}\int_{-1}^{1} \left([N_1 \;\; N_2 \;\; N_3 \;\; N_4 \;\; N_5 \;\; N_6 \;\; N_7 \;\; N_8 \;\; N_9\;] \begin{bmatrix} z_1 \\ z_2 \\ z_3 \\ z_4 \\ z_5 \\ z_6 \\ z_7 \\ z_8 \\ z_9 \end{bmatrix} \right)^2 J_{11}J_{22} - J_{12}J_{21}\,\mathrm{d}\eta\,\mathrm{d}\xi \qquad (12)$$

$$I_C = \sum_{e=1}^{2} \int_{-1}^{1}\int_{-1}^{1} \left([N_1 \;\; N_2 \;\; N_3 \;\; N_4 \;\; N_5 \;\; N_6 \;\; N_7 \;\; N_8] \begin{bmatrix} y_1 \\ y_2 \\ y_3 \\ y_4 \\ y_5 \\ y_6 \\ y_7 \\ y_8 \end{bmatrix} \right)^2 J_{11}J_{22} - J_{12}J_{21}\,\mathrm{d}\eta\,\mathrm{d}\xi \qquad (13)$$

$I_R = \frac{bd^3}{12}$

$I_C = \frac{\pi R^4}{3.9275}$

The force–displacement or stiffness characteristics of a beam element is mathematically expressed as [12]

$[k]\ \{\delta\}_e = \{P\}_e \qquad (14)$

Where

[k] = beam element stiffness matrix

$\{\delta\}_e$ = nodal displacement vector

$\{P\}_e$ = nodal force vector

[13] Derived the beam stiffness matrix based on Euler-Bernoulli's beam theory considering beam deformations only as

$$[k] = \frac{EI}{L^3}\begin{bmatrix} 12 & 6L & -12 & 6L \\ 6L & 4L^2 & -6L & 2L^2 \\ -12 & -6L & 12 & -6L \\ 6L & 2L^2 & -6L & 4L^2 \end{bmatrix} \qquad (15)$$

Where L = the span of the beam

Equation (14) can be rewritten as

$\{\delta\}_e = \{P\}_e\ [k]^{-1} \qquad (16)$

Equations (16) after some substitution, simplifications and rearrangements leads to

$$\{\delta\}_e = \{P\}_e \left(\frac{E(I_R - I_C)}{L^3} \begin{bmatrix} 12 & 6L & -12 & 6L \\ 6L & 4L^2 & -6L & 2L^2 \\ -12 & -6L & 12 & -6L \\ 6L & 2L^2 & -6L & 4L^2 \end{bmatrix} \right)^{-1} \qquad (17)$$

3.2 Analytical Load-deflection equation

The following formulas for a singly reinforced uniform rectangular section under pure bending have been obtained theoretically. When a constant bending moment (zero shearing force) acts on a length of a beam, pure bending occurs [14]. For the solid rectangular section, the moment of inertia is given by

$I_{RT} = \frac{bd^3}{12} \qquad (18)$

Where

b = width of the section

d=depth of the section

For the circular-hollow section, the moment of inertia is given by

$I_{CT} = \frac{\pi R^4}{4} \qquad (19)$

Where
R = Radius of the central hollow core.
For the circular-hollow rectangular sections, the moment of inertia is given by

$$I = \frac{bd^3}{12} - \frac{\pi R^4}{4} \quad (20)$$

Theoretically, the deflections of the beams have been calculated using the empirical formula

$$\delta = \frac{PL^3}{48EI} \quad (21)$$

Equation (21) by substitution of known values leads to

$$\delta = \frac{PL^3}{48E(\frac{bh^3}{12} - \frac{\Pi R^4}{4})} \quad (22)$$

4.0 Results and Discussions

The results are presented in figure 4.1, figure 4.2, figure 4.3, figure 4.4, figure 4.5, and figure 4.6. A plot of the failure load against hollow core diameter shown in figure 4.1 and figure 4.2, reveal that the ultimate load increased as the diameter of the hollow core increased up to 75mm, beyond which the ultimate load dropped for Type 2 Beam. A plot of the deflection against hollow core diameter shown in figure 4.3 and figure 4.4, reveal that the deflection increased as the diameter of the hollow core increased up to 30mm, beyond which the deflection dropped for all Beam type. A plot of the moment of inertia against the hollow core diameter shown in figure 4.5 and figure 4.6 reveal that the moment of inertia increased as the diameter of the hollow core increased. A very good agreement between numerical and analytical results is obtained. The flexural behavior of the hollow-cored beams for the numerical and analytical approach agreed with that of the flexural behavior investigated by [8] who experimentally and analytically investigated the flexural characteristics of Reinforced Hollow-Cored concrete beams point loaded at mid-span using the Moment of Inertia theory.

Table 4.1: Cross section of the Beam types [7]

	Type 1 Beam		Type 2 Beam		Type 3 Beam		
Diameter of Hole	Width, b (mm)	Depth, d (mm)	Width, b (mm)	Depth, d (mm)	Width, b (mm)	Depth, d (mm)	Length, L (mm)
0	150	150	150	150	150	150	750
30	150	155	155	150	152	152	750
60	150	169	169	150	159	159	750
75	150	179	179	150	164	164	750
108	150	211	211	150	178	178	750

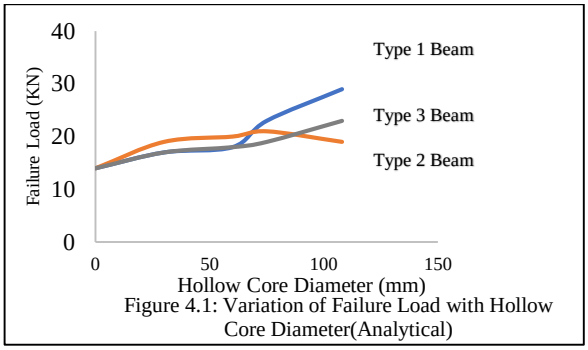

Figure 4.1: Variation of Failure Load with Hollow Core Diameter(Analytical)

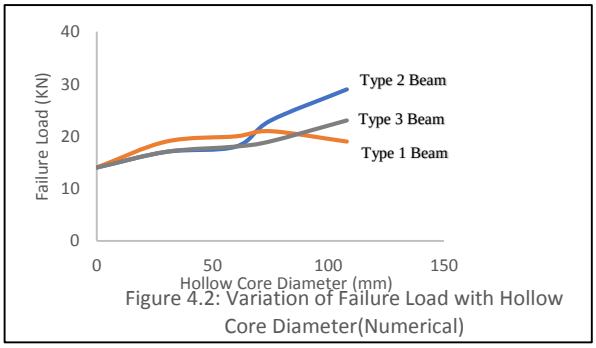

Figure 4.2: Variation of Failure Load with Hollow Core Diameter(Numerical)

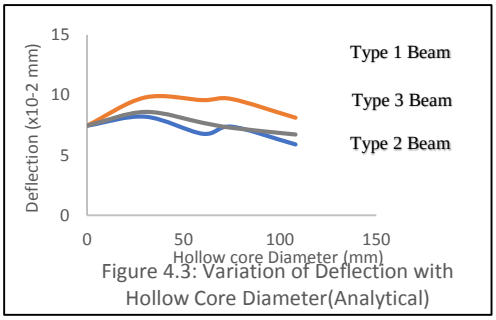

Figure 4.3: Variation of Deflection with Hollow Core Diameter(Analytical)

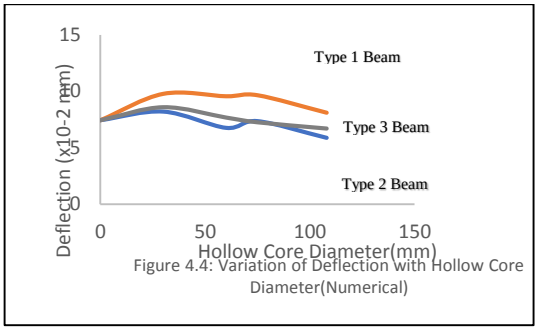

Figure 4.4: Variation of Deflection with Hollow Core Diameter(Numerical)

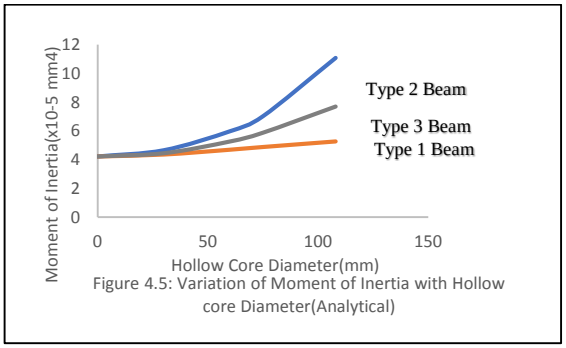

Figure 4.5: Variation of Moment of Inertia with Hollow core Diameter(Analytical)

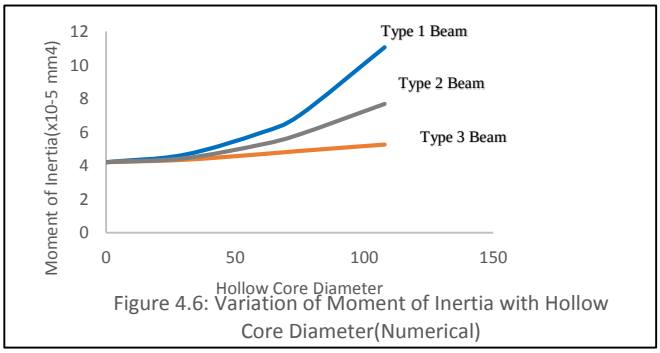

Figure 4.6: Variation of Moment of Inertia with Hollow Core Diameter(Numerical)

5.0 Conclusion

The following conclusions have been made from the study; the moment of inertia of rectangular concrete beam is increased by the introduction of a longitudinal HC for constant width and varied depths, varied width and constant depth, and varied width and varied depth. As the hole diameter increased beyond 30mm, the deflection reduced. Type 1 Beam performed best. Therefore the flexural performance of a Rectangular beam is improved by the introduction of a longitudinal circular hollow core with constant width and varied depth.

6.0 References

[1] Orie, O. E. and Idolor, B. (2015) Optimizing Compression Zone Of Flanged Hollow Cored Concrete Beams Using Moment Of Inertia Theory, Nigerian Journal of Technology (NIJOTECH). Vol. 34, Issue 2, pp. 217 – 222.

[2] Sharma, S. K. (2016) A Dissertation Report On "Finite Element Modelling Of Hollow Concrete Blocks" Submitted In Partial Fulfillment Of The Requirements For The Award Of Degree Of Master Of Technology In Structural Engineering Department Of Civil Engineering, Malaviya National Institute Of Technology, Jaipur.

[3] Al-Azzawi, A. A. and Abed, S. A. (2016) Numerical Analysis of Reinforced Concrete Hollow-Core Slabs, ARPN Journal of Engineering and Applied Sciences. Vol. 11, Issue 15, pp. 9284 – 9296.

[4] Kumbhar, U. N. and Jadhav, H. S.(2018) Flexural Behaviour Of Reinforced Concrete Hollow Beam With Polypropylene Plastic Sheet Infill, International Research Journal of Engineering and Technology (IRJET).Vol. 05, Issue 05, pp.1517-1521.

[5] Daud, S. A., Daud, R. A. and Al-Azzawi, A. A (2021) Behavior of reinforced concrete solid and hollow beams that have additional reinforcement in the constant moment zone, Ain Shams Engineering Journal. Vol.12, Issue 1, pp 31-36.

[6] Fratila, E. and Kiss, Z. (2016) Finite Element Analysis Of Hollow-Core Slabs, Journal Of Applied Engineering Sciences, Vol. 6, Issue 1, pp. 29-33.

[7] Reddaiah, P. (2017) Deriving Shape Functions for 9-Noded Rectangular Element by using Lagrange Functions in Natural Coordinate System and Verified, International Journal of Mathematics Trends and Technology (IJMTT), Vol.51, Issue 6, pp. 429 – 433.

[8] Orie, O. U. and Alutu, O. E. (2007) Flexural Characteristics of Reinforced Hollow Cored Concrete Beams Point Loaded at Mid-span, Nigerian Journal of Technological Development, Vol. 5, pp 30-38.

[9] Stasa, F. L. (1986) Applied Finite Element Analysis for Engineers, CBS Publishing -Japan Ltd.

[10] Chandrupatla, T. R. and Belegundu, A. D. (2002) Introduction to Finite Elements in Engineering, 3rd Edition. Prentice Hall, Inc. Upper Saddle River, New Jersey.

[11] Pilkey, W. D. (2002) Analysis and Design of Elastic Beams: Computational Methods, John Wiley & Sons, Inc.

[12] Bharikatti, S. S. (2005) Finite Element analysis, 1st edition, New Age International(P) ltd., New Delhi, India.

[13] Hutton, D. V. (2004) Fundamentals of Finite Element Analysis, MC-Graw Hill companies, Inc., first edition.

[14] Ryder, G. H. (1982) Strength of Materials, Macmillan Press Ltd., London.